Excited-State Structure and Delocalization in Ruthenium(II)−Bipyridine Complexes That Contain Phenyleneethynylene Substituents

Yingsheng Wang,[†] Shengxia Liu,[†] Mauricio R. Pinto,[†] Dana M. Dattelbaum,[‡] Jon R. Schoonover,[‡] and Kirk S. Schanze[†,*]

Department of Chemistry, University of Florida, P.O. Box 117200, Gainesville, Florida 32611-7200, and Los Alamos National Laboratory, Materials Science and Technology Division, MS E549, Los Alamos, New Mexico 87544

Received: August 3, 2001; In Final Form: October 4, 2001

A comprehensive photophysical study has been carried out on the two complexes $[(bpy)_2Ru(4,4'\text{-PE-bpy})]^{2+}$ and $[(bpy)_2Ru(5,5'\text{-PE-bpy})]^{2+}$ (**44Ru** and **55Ru**, respectively, where bpy = 2,2′-bipyridine and PE = phenyleneethynylene). The objective of this work is to determine the effect of the phenyleneethynylene substituents on the properties of the metal-to-ligand charge-transfer excited state. The complexes have been characterized by using UV−visible absorption, photoluminescence, and UV−visible and infrared transient absorption spectroscopy. The results indicate that the MLCT excited state is localized on the PE-substituted bpy ligands. Moreover, the photophysical data indicate that in the MLCT excited state the excited electron is delocalized into the PE substituents and the manifestations of the electronic delocalization are larger when the substituents are in the 4,4′-positions.

The photophysical properties of metal-to-ligand charge transfer (MLCT) excited states are strongly influenced by the pattern of substitution on the organic ligand that acts as the electron acceptor in the MLCT transition.[1−8] As expected on the basis of a Mulliken-type charge transfer formalism, the energy of an MLCT absorption increases as the reduction potential of the acceptor ligand shifts cathodically (i.e., as the LUMO energy increases).[9] Ligand substituent effects have been used to delineate the energy gap law correlation, wherein the nonradiative decay rate of the MLCT excited state increases as the energy of the MLCT state decreases.[1] Recently, it has also been shown that increased delocalization in the acceptor ligand decreases the nonradiative decay rate, presumably due to decreased electron-vibrational coupling in the excited state.[6,8]

We have been exploring the excited-state properties in metal-organic oligomers and polymers where the acceptor ligand for an MLCT transition is an integral part of an extended π-conjugated electronic system.[10−13] This line of investigation is being pursued in order to provide a basis for understanding the excited-state properties of more complex metal−organic π-conjugated polymers that have been used for electrooptical device applications.[14−18] Most of our work has examined oligomeric and polymeric phenyleneethynylenes that contain d^6 rhenium(I), ruthenium(II), and osmium(II) polypyridine complexes that are strongly coupled to the π-conjugated backbone.[10,11,13,19] Although much has been learned from this work, in many cases the structures of the oligomers and polymers are sufficiently complicated such that it is difficult to extract quantitative information concerning the effect of the π-conjugated system on the properties of the MLCT excited state.

To address this problem, we have carried out a detailed photophysical investigation of the relatively simple model complexes, **44Ru** and **55Ru** (Chart 1). These complexes contain the $Ru(bpy)_3^{2+}$ chromophore (bpy = 2,2′-bipyridine), but in each case one of the bpy ligands is substituted with phenyleneethynylene (PE) moieties that feature a carboxyamide substituent in the 4-position on the phenylene ring. These complexes were designed with several objectives in mind. First, we sought to determine the effect that substitution of the PE substituents has on the photophysics of the MLCT excited state in the complexes. It was anticipated that the properties of the MLCT state would be modified due to electron delocalization into the PE substituents. Second, the carboxyamide groups were included in the structures specifically as mid-IR chromophores to allow the application of time-resolved infrared spectroscopy (TRIR) to

CHART 1

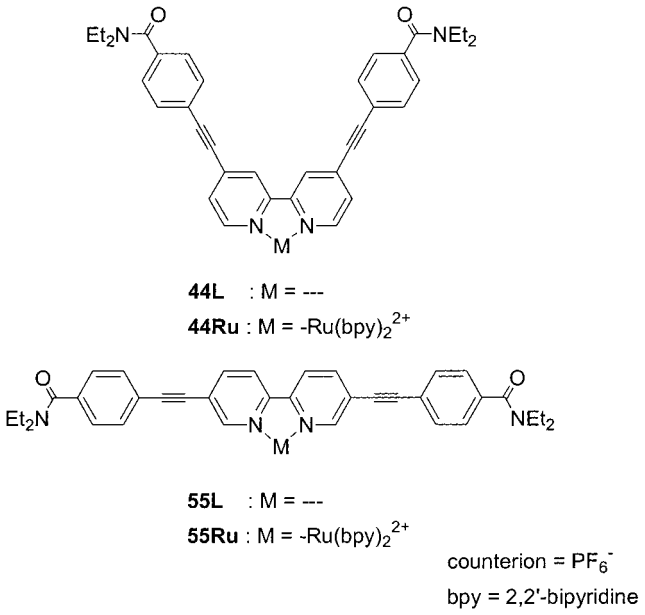

* To whom correspondence should be addressed. E-mail: kschanze@chem.ufl.edu.
[†] University of Florida.
[‡] Los Alamos National Laboratory.

10.1021/jp013008j CCC: $20.00
Published on Web 11/16/2001

probe for delocalization of the excited electron into the phenyleneethynylene unit.[20,21] The present manuscript provides a report of the photophysical properties of the complexes **44Ru** and **55Ru**. These complexes have been characterized by UV−visible absorption, photoluminescence, polarized photoluminescence as well as time-resolved UV−visible and infrared spectroscopy. The results indicate that in both cases the PE-substituted bpy is the chromophoric ligand. Although there is clear evidence from absorption, emission, and emission polarization spectroscopy for delocalization into the PE units, the effect of delocalization on the excited-state decay parameters is comparatively small.

Experimental Section

General Synthesis. Reagent grade solvents and chemicals were used for synthesis without purification unless otherwise noted. THF was distilled from Na−benzophenone. Chromatography was carried out using either silica gel (Merck, 230−400 mesh) or neutral Alumina (Fisher Chemical Company, 6% water added, Brockman grade III). NMR spectra were obtained on a Varian Gemini NMR spectrometer operating at 300 MHz. Proton NMR spectra of **44L**, **55L**, **44Ru**, and **55Ru** and electrospray mass spectra of **44Ru** and **55Ru** are available as Supporting Information.

5,5′-Bis[(4-(*N*,*N*-diethylcarboxamido)phenyl)ethynyl]-2,2′-bipyridinyl (55L). 5,5′-Diethynyl-2,2′-bipyridine[22,23] (75 mg, 0.36 mmol), 4-iodo-*N*,*N*-diethylbenzamide[24] (245 mg, 0.81 mmol), diethylamine (3 mL, 29 mmol), and THF (5 mL) were mixed in a three-necked round-bottom flask. The solution was purged with N_2 for 10 min whereupon $Pd(PPh_3)_2Cl_2$ (3.9 mg, 5.6 μmol) and CuI (1.9 mg, 9.9 μmol) were added. The solution was stirred at room temperature under N_2 for 14 h. During the course of the reaction the product precipitated from the reaction mixture as a yellow microcrystalline material. The product was isolated by filtering the reaction mixture through a medium porosity fritted funnel. The crude product was purified by washing with ether, yield 150 mg (75%). ^{1}H NMR ($CDCl_3$, 300 MHz): δ 1.13 (br, 6H), 1.25 (br, 6H), 3.27 (br, 4H), 3.54 (br, 4H), 7.40 (d, 4H), 7.60 (d, 4H), 7.96 (d, 2H), 8.45 (d, 2H), 8.82 (s, 2H).

4,4′-Bis[(4-(*N*,*N*-diethylcarboxamido)phenyl)ethynyl]-2,2′-bipyridinyl (44L). This compound was prepared according to the procedure described for **55L**, except that 4,4′-diethynyl-2,2′-bipyridine[25] was used in place of 5,5′-diethynyl-2,2′-bipyridine. The reaction mixture was concentrated under reduced pressure. The crude product was purified by column chromatography on silica gel eluting with diethyl ether:methanol (100:1 v:v). The purified product was recovered as a white solid, yield 120 mg (60%). ^{1}H NMR ($CDCl_3$, 300 MHz): δ 1.14 (br, 6H), 1.26 (br, 6H), 3.28 (br, 4H), 3.56 (br, 4H), 7.40 (d, 4H), 7.43 (d, 2H), 7.60 (d, 4H), 8.55 (s, 2H), 8.70 (d, 2H).

55Ru. $Ru(bpy)_2Cl_2$[26] (70 mg, 0.135 mmol), $AgCF_3SO_3$ (138 mg, 0.54 mmol), and acetone (15 mL) were combined in a round-bottom flask. The solution was refluxed under N_2 for 2 h. TLC (silica, CH_2Cl_2:MeOH, 5:1 v:v) of the reaction mixture shows a spot with $R_f = 0.15-0.25$, which is believed to be the product, $Ru(bpy)_2(CF_3SO_3)_2$. The reaction mixture was filtered through a medium porosity fritted funnel and the filtrate was concentrated to a volume of 3−4 mL. The concentrated $Ru(bpy)_2(CF_3SO_3)_2$/acetone solution was transferred to a clean round-bottom flask, whereupon **55L** (96 mg, 0.173 mmol) and 95% EtOH (14 mL) were added. The resulting solution was refluxed under N_2 for 17 h. The reaction mixture was cooled and then an aqueous solution of NH_4PF_6 (450 mg, 10 mL) was added. The product precipitated as a brick-red powder. The crude product was collected by filtration, washed with diethyl ether, and then purified by column chromatography on alumina eluting with mixtures of CH_2Cl_2 and CH_3CN (gradient, CH_2Cl_2:CH_3CN from 10:1 to 10:4 v:v). The collection was monitored by UV−visible spectroscopy. The product-containing fractions were combined and concentrated to dryness. The chromatographed product was reprecipitated by dropping a concentrated CH_2Cl_2 solution into excess diethyl ether and it was collected by filtration. The final product was obtained as a brick-red microcrystalline solid, yield 90 mg (50%). ^{1}H NMR (CD_3CN, 300 MHz): δ 1.05 (br, 6H), 1.18 (br, 6H), 3.18 (br, 4H), 3.45 (br, 4H), 7.36 (d, 4H), 7.41 (q, 4H), 7.51 (d, 4H), 7.69 (d, 2H), 7.80 (d, 2H), 7.85 (d, 2H), 8.07 (q, 4H), 8.15 (dd, 2H), 8.49 (s, 2H), 8.50 (dd, 4H). HRMS (electrospray, FT-MS): Calcd for $C_{56}H_{50}O_2N_8F_6PRu$: 1113.275. Found: 1113.303. The full HRMS along with calculated isotope distribution is available as Supporting Information.

44Ru. This compound was prepared according to the procedure described for **55Ru**, except that **44L** was used in place of **55L**. The crude product was purified by column chromatography on alumina eluting with CH_2Cl_2:CH_3CN (4:1 v:v). The collection was monitored by UV−visible spectroscopy. The product-containing fractions were combined and concentrated to dryness. The chromatographed product was reprecipitated by dropping a concentrated CH_2Cl_2 solution into excess diethyl ether, and it was collected by filtration. The final product was obtained as a brick-red microcrystalline solid, yield 50%. ^{1}H NMR (CD_3CN, 300 MHz): δ 1.1 (br, 6H), 1.2 (br, 6H), 3.2 (br, 4H), 3.5 (br, 4H), 7.4 (m, 10H), 7.7 (m, 10H), 8.07 (m, 4H), 8.5 (d, 4H), 8.65 (s, 2H). HRMS (electrospray, FT-MS): Calcd for $C_{56}H_{50}O_2N_8F_6PRu$: 1113.275. Found: 1113.304. The full HRMS along with calculated isotope distribution is available as Supporting Information.

Spectroscopy and Electrochemistry. UV−visible absorption spectra were obtained on a Varian Cary 100 spectrophotometer. Corrected steady-state emission spectra were recorded on a SPEX F-112 fluorescence spectrometer. Samples were contained in 1 cm × 1 cm quartz cuvettes, and the optical density was adjusted to approximately 0.1 at the excitation wavelength. Emission quantum yields are reported relative to $[Ru(bpy)_3^{2+}]$-$[Cl^-]_2$ in water ($\Phi_{em} = 0.055$)[27] and appropriate correction was applied for the difference in refractive indices of the sample and actinometer solvents.[28] Low-temperature fluorescence experiments were carried out by cooling the samples in an Oxford Instruments DN-1704 optical cryostat. Samples for low-temperature spectroscopy were dissolved in an ethanol/methanol (4:1 v:v) solvent mixture. Time-resolved emission decays were obtained by time-correlated single photon counting on an instrument that was constructed in-house. Excitation was effected by using a blue diode laser (IBH instruments, Edinburgh, Scotland, pulse width 800 ps). The time-resolved emission was collected using a red-sensitive, photon-counting PMT (Hamamatsu R928) and the light was filtered using 10 nm band-pass interference filters. Lifetimes were determined from the observed decays with the DAS6 deconvolution software (IBH instruments, Edinburgh, Scotland). Nanosecond transient absorption spectra were obtained on previously described instrumentation,[29] with the third harmonic of a Nd:YAG laser (355 nm, 10 ns fwhm, 5 mJ pulse^{-1}) as the excitation source. Time-resolved infrared spectroscopy was carried out on a step-scan FTIR instrument that has been previously described.[30,31] Samples were dissolved in CH_3CN and were purged

with Ar. Excitation was effected using the third harmonic output of a Nd:YAG laser (355 nm).

The emission spectra were fitted using a single-mode Franck−Condon expression (eq 1a),

$$I(\bar{\nu}) = \sum_{\nu_m=0}^{5}\left\{\left(\frac{E_{00} - \nu_m\hbar\omega_m}{E_{00}}\right)^3 \frac{(S_m)^{\nu_m}}{\nu_m!} \exp\left[-4\ln 2\left(\frac{\bar{\nu} - E_{00} + \nu_m\hbar\omega_m}{\Delta\bar{\nu}_{0,1/2}}\right)^2\right]\right\} \quad (1a)$$

$$S = 1/2(M\omega/\hbar)(\Delta Q_e)^2 \quad (1b)$$

where $I(\bar{\nu})$ is the relative emission intensity at energy $\bar{\nu}$, E_{00} is the energy of the zero-zero transition, ν_m is the quantum number of the average medium-frequency vibrational mode, $\hbar\omega_m$ is the average of medium-frequency acceptor modes coupled to the MLCT transition (1300 cm^{-1} was assumed throughout the series), S_m is the Huang−Rhys factor (i.e., the electron-vibration coupling constant), and $\Delta\bar{\nu}_{0,1/2}$ is the half-width of the individual vibronic bands. S_m is related to the difference in equilibrium displacement for the normal modes (ΔQ_e) between the ground and excited state by eq 1b. In eq 1b, M is the reduced mass and ω is the angular frequency.

Polarized photoluminescence excitation spectroscopy was carried out on a SPEX F-112 fluorescence spectrometer that was fitted with Glans-Thompson polarizers (single-channel, right angle format).[32] Samples were dissolved in ethanol/methanol (4:1 v:v) and cooled to 80 K in the DN-1704 optical cryostat. Wavelength-resolved polarization anisotropies, $r(\lambda)$, were computed according to the following equation,

$$r(\lambda) = \frac{I_{VV}(\lambda) - GI_{VH}(\lambda)}{I_{VV}(\lambda) + 2GI_{VH}(\lambda)} \quad (2)$$

where G is $I_{HV}(\lambda)/I_{HH}(\lambda)$ and $I_{xy}(\lambda)$ is the emission intensity at wavelength λ with the excitation and emission polarizers adjusted according to x and y, respectively. (For example, I_{HV} is the emission intensity with horizontally polarized excitation and vertically polarized emission.) Four separate excitation scans were required to obtain the necessary intensity arrays, $I_{VV}(\lambda)$, $I_{VH}(\lambda)$, $I_{HV}(\lambda)$, and $I_{HH}(\lambda)$. These four intensity arrays were imported into an Excel spreadsheet that was used to compute $r(\lambda)$ according to eq 2.

Electrochemical measurements were conducted on CH_3CN solutions with tetrabutylammonium hexafluorophosphate (TBAH, Aldrich) as the supporting electrolyte. Cyclic voltammetry was carried out on nitrogen bubble-degassed solutions (TBAH = 0.1 M) with a BAS CV-27 voltammograph and MacLab Echem software. A platinum disk working electrode, platinum wire auxiliary electrode, and silver wire quasi-reference electrode were used, and potentials were corrected to values vs SCE via an internal standard (ferrocene, $E_{1/2}(Fc^+/Fc) = +0.40$ V vs SCE).[33,34] A scan rate of 100 mV s^{-1} was employed in all measurements.

Calculations were carried out using the Gamess client software[35] running through the Chem 3D (Cambridge Software) interface. The ligand structures were geometry optimized by using Hartree−Fock SCF theory with an STO 3G basis set. In the optimized structures of both ligands, the 2,2′-bipyridine unit was in the s-cis conformation and all of the aryl rings were in the *xy* plane.

TABLE 1: Electrochemical Potentials[a]

complex	$E_{1/2}^{ox}$/V	$E_{1/2}^{red}$/V
$Ru(bpy)_3^{2+}$	+1.30 ($Ru^{II/III}$)	−1.34 ($bpy^{0/\bullet-}$)
		−1.53 ($bpy^{0/\bullet-}$)
		−1.79 ($bpy^{0/\bullet-}$)
4,4′-Ru	+1.33 ($Ru^{II/III}$)	−1.11 (**44L**$^{0/\bullet-}$)
		−1.46 ($bpy^{0/\bullet-}$)
		−1.71 ($bpy^{0/\bullet-}$)
5,5′-Ru	+1.35 ($Ru^{II/III}$)	−0.97 (**55L**$^{0/\bullet-}$)
		−1.42 ($bpy^{0/\bullet-}$)
		−1.58 ($bpy^{0/\bullet-}$ or **55L**$^{\bullet-/2-}$)

[a] Potentials in CH_3CN/0.1 M tetrabutylammonium perchlorate solution, Pt disk working electrode, Pt wire auxiliary electrode, Ag/AgCl quasi-reference electrode. Potentials were calibrated by using a ferrocene internal standard and are converted to SCE by assuming $E_{1/2}(Fc^+/Fc) = +0.40$ V vs SCE.[33,34]

Results and Discussion

Electrochemistry. Cyclic voltammetry was carried out on the PE-substituted metal complexes **44Ru**, **55Ru**, and on $Ru(bpy)_3^{2+}$. Potentials for the first oxidation and first three reduction waves for the three complexes are listed in Table 1. Each complex features an anodic wave in the 1.30−1.35 V region due to the $Ru^{II/III}$ couple. This wave is shifted to slightly more positive potentials in **44Ru** and **55Ru** due to the effect of the PE substituents that exert an electron-withdrawing effect on the bipyridine. All of the complexes feature three well-resolved, reversible cathodic waves. For **44Ru**, the first reduction occurs at −1.11 V; this wave clearly arises from reduction of the coordinated **44L**. The +240 mV shift of the ligand-centered reduction (relative to the first reduction of $Ru(bpy)_3^{2+}$) indicates that the PE substituents lower the LUMO energy of **44L** relative to bpy. The second and third cathodic waves in **44Ru** occur at slightly more positive potentials compared to those for the corresponding waves in $Ru(bpy)_3^{2+}$. Nevertheless, given the reasonable correspondence between the potentials for these waves, it is likely that the second and third waves for **44Ru** arise from reduction of the ancillary bpy ligands. For **55Ru**, the first cathodic wave is shifted to an even more positive potential (+370 mV relative to $Ru(bpy)_3^{2+}$), indicating that the substituent effect of the PE groups is stronger when they are in the 5,5′-positions. The second and third cathodic waves in **55Ru** are also shifted to more positive potentials. While it is likely that for this complex the second cathodic wave arises from reduction of an ancillary bpy ligand, it is possible that the third reduction corresponds to a second one-electron reduction of the coordinated **55L**.

Several conclusions can be drawn from the electrochemistry of the PE-substituted complexes. First, it is clear that the PE groups lower the LUMO energy in the substituted bpy ligands. The effect is more pronounced in **55Ru**, consistent with previous studies which show that electron-withdrawing substituents exert a greater stabilizing effect on the LUMO energy when they are in the 5,5′-positions.[2] Although it is unclear how the PE substituents act to stabilize the LUMO in **44L** and **55L**, molecular orbital calculations of PE-substituted 2,2-bipyridines suggest that the effect arises from orbital delocalization into the PE substituents (vide infra).[36,37] Second, in a recent study Swager and co-workers reported the electrochemical properties of a series of tris(2,2′-bipyridine) complexes in which the ligands were substituted in the 4,4′- and 5,5′-positions with bithiophene (BT) moieties.[38] By analogy with the present work, the BT substituents stabilize the LUMO of the substituted bpy ligands and the effect is larger when the BT groups are in the 5,5′-

TABLE 2: Photophysical Properties of Ru Complexes[a]

complex	λ_{max}^{abs}/nm	$\epsilon_{max}/10^3$ M^{-1} cm^{-1}	assignment	λ_{max}^{em}/nm	Φ_{em}	τ_{em}, μs	τ_{TA}/μs	$k_r/10^5$ s^{-1}	$k_{nr}/10^5$ s^{-1}
44Ru	482	19.3	Ru → **44L** MLCT	668	0.16	1.4	1.3	1.1	6.0
	445	16.1	Ru → bpy MLCT						
	402	14.0							
	367	20.2							
	315	49.2	π,π^* **44L**						
	287	79.0	π,π^* bpy						
55Ru	490(sh)	7.4	Ru → **55L** MLCT	693	0.035	0.52	0.45	0.67	18
	442	10.0	Ru → bpy MLCT						
	366	68.9	π,π^* **55L**						
	330	46.5							
	287	76.0	π,π^* bpy						

[a] Argon degassed CH_3CN solution.

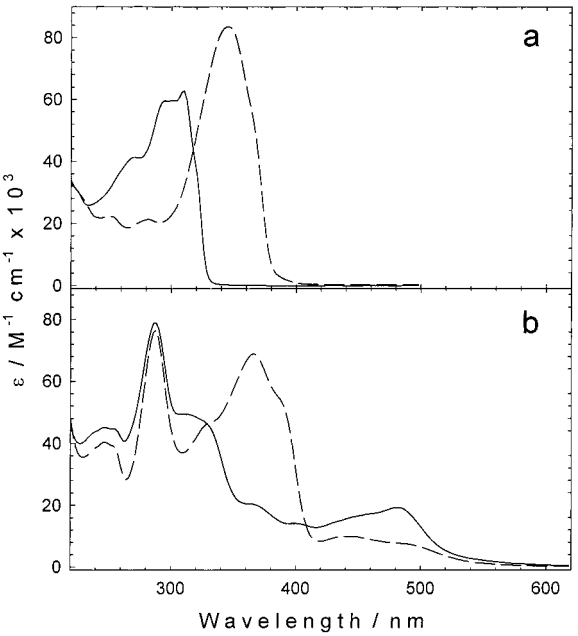

Figure 1. UV−visible absorpton spectra in CH3CN solutions: (a) (−) **44L**, (- - -) **55L**; (b) (−) **44Ru**, (- - -) **55Ru**.

positions. However, the BT substituents have a significantly smaller effect on the LUMO energy compared to the PE substituents.

UV−Visible Absorption Spectroscopy. UV−visible absorption spectra were recorded for the free ligands **44L** and **55L** in $CHCl_3$ and for metal complexes **44Ru** and **55Ru** in CH_3CN. Figure 1 shows the spectra, and Table 2 provides a tabular listing of the absorption bands and band assignments in the metal complexes. The free ligands display relatively intense absorption in the UV region. In **55L**, which features a "linear" geometry, the predominant band is shifted to lower energy and is more intense compared to the absorption of **44L**. The predominant absorption in **55L** arises from the long-axis polarized π,π^* absorption of the "oligomer". This absorption is very similar in intensity, band shape, and energy to the absorption of linear oligomeric phenyleneethynylenes (OPEs) that have been previously reported.[11,13,39,40] In addition to being blue-shifted and less intense, the absorption of **44L** is more structured. The blue shift likely arises due to disruption in the long-axis conjugation that arises due to the 4,4′-pattern of substitution on the bpy moiety (i.e., with respect to the π-conjugated system, this molecule is 1,3- or "meta" linked).

As might be expected, the absorption spectra of the metal complexes **44Ru** and **55Ru** are considerably more complex than compared to the free ligand counterparts. In addition to the intraligand bands that occur in the UV region, the metal complexes feature a manifold of MLCT transitions in the visible region. First, **55Ru** features two prominent absorptions in the UV: a narrow band at 287 nm arising from the π,π^* absorption of the ancillary bpy ligands and a second broader band at 366 nm that is due to the long-axis polarized π,π^* absorption of the coordinated **55L**. Note that the π,π^* absorption of **55L** is red-shifted in the complex relative to its position in the free ligand. Similar behavior has been observed for other π-conjugated bipyridine ligands, and the effect has been attributed to the effect of the (electrophilic) metal center on the energies of the π and π^* levels of the ligand.[13,38,41] In the visible region, **55Ru** features a broad MLCT absorption that appears to consist of at least two overlapping bands, one at 442 nm and the second at 490 nm. We assign the low-energy band to the dπ (Ru) → π^* (**55L**) MLCT transition and the higher energy band to the dπ (Ru) → π^* (bpy) MLCT transition. These assignments are substantiated by the photoluminescence excitation polarization spectroscopy described below.

In complex **44Ru**, the UV absorption is dominated by the π,π^* transitions of the bpy ligands. The π,π^* transition of the coordinated **44L** appears as a shoulder on the red side of the bpy absorption. The MLCT band, which is in the visible region, is considerably more intense compared that of **55Ru**. It consists of a strong band at 482 nm with a possible second band that appears as a shoulder at 445 nm. The low-energy band is assigned to the dπ (Ru) → π^* (**44L**) MLCT transition, while the higher energy band is attributed to the π (Ru) → π^* (bpy) MLCT transition.

The enhanced oscillator strength in the dπ (Ru) → π^* (**44L**) MLCT transition likely arises because of orbital delocalization into the PE-substituents. This premise is supported by previous studies of MLCT transitions in aryl- and PE-substituted diimine metal complexes. The effect of orbital delocalization on the intensity of MLCT transitions was first noted by McMillin and Pfifer in a study of a series of Cu(I)−phenanthroline complexes.[42] These authors applied Mulliken charge transfer theory to analyze the MLCT absorption of the Cu(I) complexes, and their results showed that when the charge-transfer distance is increased due to orbital delocalization in the acceptor ligand, the oscillator strength of the MLCT transition increases.[42] We recently reported a related study on a Re(I) complex that contains PE substituents in the 4,4′-positions of a bpy ligand and concluded that the effective charge-transfer distance in the MLCT transition is increased by more than 50% due to delocalization of the excited electron into the PE substituents.[36]

Photoluminescence Spectroscopy. Free ligands **44L** and **55L** feature a strong fluorescence in the near-UV region that arises from the π,π^* state with λ_{max} at 350 and 385 nm, respectively. In the metal complexes the fluorescence is quenched, and it is

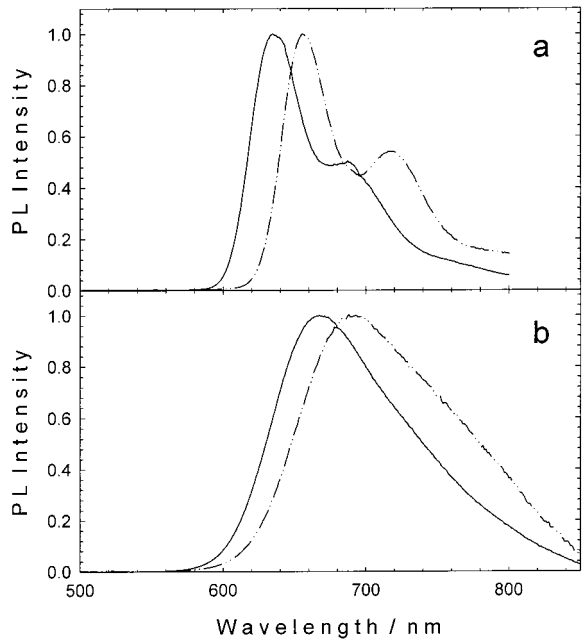

Figure 2. Intensity normalized photoluminescence spectra of **44Ru** (−) and **55Ru** (- - -): (a) 80 K, ethanol/methanol (4:1 v:v) glasses; (b) 298 K, CH_3CN solutions.

TABLE 3: Emission Spectral Fitting Parameters[a]

complex	T/K	E_{00}/cm^{-1}	$\hbar\omega_m$/cm^{-1}	S_m	$\Delta\bar{\nu}_{0,1/2}$/cm^{-1}
44Ru	298	15100	1200	0.7	1500
44Ru	80	15700	1200	0.7	1000
55Ru	298	14500	1300	0.85	1450
55Ru	80	15200	1300	0.85	1000

[a] Ethanol/methanol (4:1 v:v) solvent.

replaced by a red photoluminescence (PL). The PL spectra of the complexes obtained in CH_3CN at 298 K and in ethanol/methanol (4:1 v:v) at 80 K are illustrated in Figure 2. At room temperature, the PL from the complexes appears as a broad band with $\lambda_{max} = 668$ (**44Ru**) and 693 nm (**55Ru**) (Figure 2b). At 80 K, the emission from both complexes is blue-shifted and appears as a broad manifold with a clearly resolved vibronic progression (Figure 2a). The red PL is clearly due to the MLCT excited states for both complexes. The MLCT assignment is supported by the PL decay lifetimes, which are 1.4 and 0.52 μs (298 K in CH_3CN), for **44Ru** and **55Ru**, respectively. The blue shift that occurs upon cooling is due to the rigidochromic effect, which is well-documented for MLCT PL in transition metal complexes.[43,44]

To extract information concerning the structure of the luminescent excited states from the PL data, the spectra were fitted using a single-vibrational mode Franck−Condon band shape expression (eq 1, see Experimental Section). The fits were first carried out on the 80 K spectra and in this procedure all four fitting parameters (E_{00}, $\hbar\omega_m$, S_m, and $\Delta\bar{\nu}_{0,1/2}$) were varied to optimize the fits. The room temperature spectra were subsequently fitted. In this case the parameters S_m and $\hbar\omega_m$ were set to the values recovered from the 80 K fitting procedure, and the fits were optimized by varying only E_{00} and $\Delta\bar{\nu}_{0,1/2}$. The parameters recovered from the fitting procedure are listed in Table 3, and the fitted spectra are available as Supporting Information.

Several points are of interest with respect to the parameters recovered from the fits. First, in both cases in the 80 K spectra there is a clearly resolved vibrational progression arising from C−C modes of the PE-substituted bpy ligands. Second, the Huang−Rhys parameters (S_m) that are recovered from the 80 K fitted spectra indicate that in both complexes the electron-vibrational coupling in the MLCT excited state is comparatively low. This feature is quite clear from the appearance of the low-temperature emission spectra, where the intensity of the 0,1 transition is considerably less intense compared to that of the 0,0 band. (For comparison, S_m for $Ru(bpy)_3^{2+}$ is ∼0.95).[28] Third, S_m is greater for **55Ru** than for **44Ru**, despite the fact that the energy of the MLCT state is larger for the latter complex. This runs counter to expectation, since theory and experimental evidence indicate that S_m typically *increases* with E_{00}.[45] Based on the fact that S_m(**44Ru**) < S_m(**55Ru**), we tentatively conclude that in the MLCT state the excited electron is more delocalized in **44Ru**. This point is discussed at more length in a later section.

Excited-State Decay Kinetics. In many Ru(II)−polypyridine complexes, the decay kinetics of the MLCT state are complicated by the existence of a metal-centered (dd) excited state that is in close energetic proximity to the luminescent MLCT state.[46,47] The existence of the dd state is typically inferred from the observation of a moderately strong temperature dependence in the MLCT decay kinetics.[47] This temperature dependence arises from thermally activated MLCT → dd internal conversion (IC). However, when the MLCT state is at a comparatively low energy, thermally activated MLCT → dd IC is slower than the normal radiative and nonradiative decay channels and, consequently, the MLCT decay kinetics are relatively temperature independent.[47] In this case, the ambient temperature emission decay lifetime (τ_{em}) and emission quantum yield (ϕ_{em}) provide reasonable estimates for the intrinsic radiative and nonradiative decay rates (k_r and k_{nr}, respectively) of the MLCT excited state according to eqs 3 and 4,

$$k_r = \phi_{em}/\tau_{em} \quad (3)$$

$$k_{nr} = (1 - \phi_{em})/\tau_{em} \quad (4)$$

Given the relatively low energy of the MLCT state in **44Ru** and **55Ru**, it was anticipated that at ambient temperature thermally activated MLCT → dd IC would not be competitive with the normal excited-state decay channels. To confirm this premise, the temperature dependence of τ_{em} for the two complexes was determined in CH_3CN solution over the temperature range 235−295 K. For both complexes over this temperature range τ_{em} varied by less than 10% (see Table in Supporting Information). In view of this result we conclude that reasonably accurate k_r and k_{nr} values can be computed from the ambient temperature τ_{em} and ϕ_{em} values. Thus, the τ_{em} and ϕ_{em} values for **44Ru** and **55Ru** determined at ambient temperature in CH_3CN solution were used to compute k_r and k_{nr} values according to eqs 3 and 4 (see Table 2 for values).

There are several noteworthy features with respect to the photophysical parameters of the PE-substituted complexes. First, both τ_{em} and ϕ_{em} are considerably larger for **44Ru**. This trend is consistent with the energy gap law: since E_{00} is larger for **44Ru**, one would expect k_{nr} for this complex to be lower (τ_{em} and ϕ_{em} increase as k_{nr} decreases).[1,48] However, inspection of the k_r and k_{nr} values for **44Ru** and **55Ru** indicates that the considerably enhanced ϕ_{em} for **44Ru** arises not only because k_{nr} is smaller but also because k_r is larger. This finding indicates that radiative decay is enhanced when the PE substituents are in the 4,4′-positions. This is consistent with a previous study by McCusker that examined a series of aryl-substituted Ru−polypyridine complexes in which the aryl groups were in the 4,4′-positions of the bpy ligands.[8] In this study it was seen that

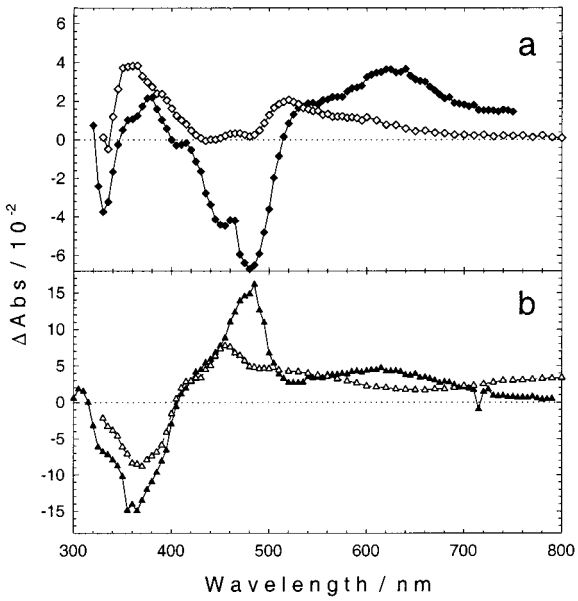

Figure 3. Transient absorption-difference spectra for **44Ru** and **55Ru** in CH_3CN solution: (a) **44Ru** and (b) **55Ru**. Legend: (filled symbols) complex alone, $c = 2 \times 10^{-5}$ M; (unfilled symbols) complex, $c = 2 \times 10^{-5}$ M, and dimethylaniline, $c = 30$ mM. Spectra are the principal components extracted from factor analysis of time-resolved absorpton spectral data. The principal component spectra are normalized to correspond to ΔA at time 0.

k_r increased systematically as the degree of delocalization into the aryl subsitutent increased. The authors concluded that the radiative decay rate is enhanced because the transition dipole moment, $\vec{\mu}$, is increased by orbital delocalization into the 4,4′-aryl substituents.[8] We conclude that a similar effect is operative in **44Ru**; that is, $\vec{\mu}$ for the MLCT state is enhanced by delocalization into the 4,4′-PE substituents.

UV−Visible Transient Absorption Spectroscopy. Laser flash photolysis was carried out on **44Ru** and **55Ru** in order to obtain information concerning the (difference) absorption spectra of the MLCT excited state. The transient absorption (TA) difference spectra of **44Ru** and **55Ru** in degassed CH_3CN solution following 355 nm excitation are illustrated in Figure 3 (filled polygons) and the TA decay lifetimes are listed in Table 2. As expected, both complexes feature comparatively strong transient absorption, and on the basis of the correspondence between the TA and emission decay lifetimes, the TA difference spectra are assigned to the MLCT excited states.

The TA difference spectrum of **44Ru** is characterized by moderately strong absorption in the near-UV, strong ground-state bleaching in the 400−500 nm region, and broad, moderate absorption for $\lambda > 500$ nm. It is noteworthy that the TA difference spectrum of **44Ru** is qualitatively similar to that of $Ru(bpy)_3^{2+}$,[49] and it has been shown that for the latter the principal TA bands arise from intraligand (IL) absorptions due to the reduced bpy ligand in the excited state.[50] By analogy we suggest that the principal TA features for **44Ru** arise due the reduced 4,4′-PE substituted ligand that is present in the excited-state complex, $[(bpy)_2Ru^{III}(\mathbf{44L}^{\bullet-})]^{2+}*$.

The TA difference spectrum of **55Ru** is distinct from that of **44Ru**. First, qualitatively the TA of **55Ru** is considerably stronger than that of **44Ru**,[51] which suggests that the ground−excited-state difference absorptivity ($\Delta\epsilon$) is larger in the former complex. The TA difference spectrum of **55Ru** features strong bleaching at $\lambda \approx 360$ nm and strong absorption at $\lambda \approx 490$ nm. Interestingly, in this complex the bleaching occurs in the ground-state absorption band that is assigned to the π,π^* transition of **55L**, rather than in the region of the MLCT absorption (400−500 nm). The lack of bleaching in the ground-state MLCT bands is believed to be due to the fact that the excited-state absorption is very strong in this region (i.e., $\Delta\epsilon$ is large and positive, which offsets any bleaching due to the loss of absorptivity in the MLCT bands). It is believed that the principal TA absorption features observed for excited state **55Ru** arise from to the reduced 5,5′-PE substituted ligand, i.e., $[(bpy)_2Ru^{III}(55L^{\bullet-})]^{2+}*$. The strong visible absorption band in the excited state apparently arises from the $\pi^*-\pi^*$ transitions for $\mathbf{55L}^{\bullet-}$; it is likely that because of the strong conjugation in this ligand, the absorptivity of the radical anion is large.

The dominant TA spectral features of MLCT excited states arise from the absorbance of the reduced acceptor ligand.[50,52,53] In the foregoing analysis of the TA spectra of **44Ru** and **55Ru**, a similar argument is invoked to support the TA difference spectral assignments. To provide further evidence in support of the premise that the principal TA spectral features observed for the MLCT states of **44Ru** and **55Ru** arise from the reduced PE-substituted ligands, laser flash photolysis experiments were carried out with **44Ru** and **55Ru** in CH_3CN solution with the reductive quencher *N*,*N*′-dimethylaniline (DMA). Under these conditions, photoexcitation of the complexes affords the one-electron reduced complexes in moderate to high yield,[54]

$$[(bpy)_2Ru^{II}(\mathbf{55L})]^{2+} + DMA \xrightarrow{h\nu} [(bpy)_2Ru^{II}(\mathbf{55L}^{\bullet-})]^{+} + DMA^{\bullet+} \quad (5)$$

$$[(bpy)_2Ru^{II}(\mathbf{44L})]^{2+} + DMA \xrightarrow{h\nu} [(bpy)_2Ru^{II}(\mathbf{44L}^{\bullet-})]^{+} + DMA^{\bullet+} \quad (6)$$

Since $DMA^{\bullet+}$ absorbs only moderately in the visible region,[55] under the conditions of these experiments the principal TA features are expected to arise from the difference in absorption of the corresponding ground state and one-electron-reduced complexes. Figure 3 illustrates the TA difference spectra of **44Ru** and **55Ru** obtained in CH_3CN solution with [DMA] = 30 mM (unfilled polygons). For both complexes, there is a clear similarity in the difference spectra of the reduced complexes and the MLCT excited states. For example, both reduced and excited state **44Ru** display an absorption band in the near-UV; as noted above, this spectral feature is characteristic of the 2,2′-bipyridine anion radical. The similarity between the absorption of the excited state and reduced complexes is especially strong in the case of **55Ru**. This underscores the fact that the reduced ligand **55L** features a strong visible absorption, and this absorption dominates the spectra of the reduced and excited-state complexes.

Emission Excitation Polarization Spectroscopy. Emission excitation spectroscopy was carried out on the PE-substituted complexes in order to obtain additional insight concerning the nature of the transitions observed in the near-UV and visible spectral regions. These experiments were carried out with the samples dissolved in an ethanol/methanol solvent glass at 80 K in order to prevent depolarization due to rotational diffusion.

In these experiments the emission anisotropy as a function of excitation wavelength, $r(\lambda_{ex})$ was determined. The anisotropy provides a measure of the angular displacement (β) between the transition moments for the absorbing and emitting states.[32] Specifically, when $\beta = 0°$ (the transition moments for the two states are parallel), $r = 0.4$ (the theoretical maximum), and when

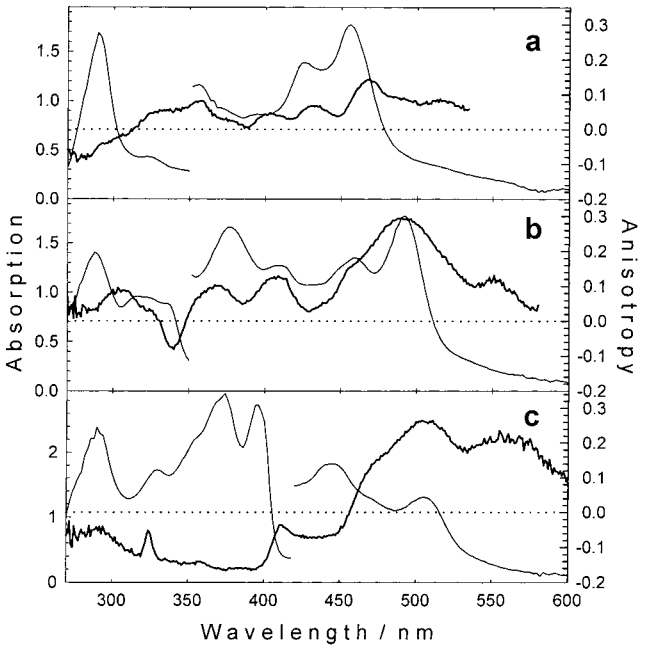

Figure 4. Absorption (fine lines, scale at left) and excitation anisotropy (bold lines, scale at right) spectra obtained at 80 K on samples in ethanol/methanol (4:1 v:v) glass: (a) $Ru(bpy)_3^{2+}$; (b) **44Ru**; (c) **55Ru**.

$\beta = 90°$ (the transition moments are perpendicular), $r = -0.2$. Intermediate values of r are observed when β is between 0 and 90°.[32]

Figure 4 illustrates absorption spectra obtained at 80 K along with the excitation polarization spectra of $Ru(bpy)_3^{2+}$ and the PE-substituted complexes.[56] The excitation polarization spectrum for $Ru(bpy)_3^{2+}$ is provided to allow comparison with the data for the PE-substituted complexes. Our data for $Ru(bpy)_3^{2+}$ are consistent with previous reports;[57] the complex features a maximum r value of ≈0.15 when the excitation wavelength corresponds to the lowest MLCT transition. The fact that $r <$ 0.4 is believed to be due to the fact that although initial excitation produces a state that is localized on a single bpy ligand, randomization from the original ligand-localized state occurs prior to light emission. This randomization results in emission from a population in which some molecules have their emission dipoles displaced significantly from the absorption dipole.[57]

Next we turn to consider the low-temperature absorption and excitation polarization spectra of **44Ru** and **55Ru**. First, the low-temperature absorption spectra of both complexes feature improved resolution in all of the transitions. For both complexes the MLCT transitions in the 400−520 nm region are clearly resolved into two bands. In each case the lowest energy band is due to the Ru → **44L** (or **55L**) transition, while the higher energy band arises from the Ru → bpy transition. The IL bands in the near-UV are also better resolved at 80 K.

The excitation polarization spectrum of **44Ru** features $r \approx$ 0.3 in the lowest energy MLCT band. The comparatively large anisotropy signals that the absorption and emission dipoles are nearly collinear ($\beta \approx 20°$) in this transition. Moreover, the large anisotropy confirms that emission occurs almost exclusively from an MLCT state that is localized on the PE-substituted ligand, i.e., the emitting state is best described as $(bpy)_2Ru^{III}$-$(\mathbf{44L}^{\bullet-})^{2+*}$. The anisotropy decreases for $\lambda_{ex} <$ 450 nm because the transition dipoles for the Ru → bpy transitions are not parallel to that of the emitting state (i.e., Ru → **44L**). An interesting point is that $r \approx -0.1$ on the red edge of the absorption band that is assigned to the **44L** IL transition. This feature implies that the lowest energy π,π^* IL transition for **44L** is polarized along the long axis of the PE-substituted 2,2-bipyridine moiety.

In the low-energy region the excitation polarization spectrum of **55Ru** is similar to that of **44Ru**. The r value for the lowest energy MLCT band is also ≈0.3 ($\beta \approx 20°$), which underscores the fact that the lowest energy absorption and the emission both occur from a state that is localized on the PE-substituted ligand. Interestingly, for **55Ru** at higher excitation energies $r < 0$. At excitation wavelengths that correspond to the π,π^* IL transition of **55L** ($\lambda = 350-400$ nm), $r \approx -0.15$, which implies that the absorbing and emitting transition dipoles are almost perpendicular ($\beta \approx 75°$). This is consistent with the hypothesis that the intense IL absorption band corresponds to the long-axis polarized π,π^* transition, which is oriented perpendicular to that of the Ru → **55L** MLCT transition.

Time-Resolved Infrared Spectroscopy. As noted in the Introduction, one objective of this project was to use time-resolved infrared spectroscopy (TRIR) to probe for excited-state delocalization in **44Ru** and **55Ru**.[58] This idea was based on TRIR experiments carried out by Meyer and co-workers on the complexes $[Ru(bpy)_2(4,4'\text{-}(CO_2Et)_2bpy)]^{2+}$ and $[Ru(bpy)_2(4,4'\text{-}(CONEt_2)_2bpy)]^{2+}$ in which one of the 2,2′-bipyridine ligands is substituted with carboxyester and carboxyamide groups.[20] In this study it was observed that in the MLCT excited state the frequency of the C═O stretching modes ($\nu_{C=O}$) of the ester and amide functional groups decreased due to the increased electron density in the acceptor bpy ligand. The frequency shifts ($\Delta\nu_{C=O}$) were −15 and −25 cm^{-1} for the amide- and ester-substituted complexes, respectively.

By analogy to this work, we anticipated that it might be possible to observe shifts in $\nu_{C=O}$ for the diethylamide substituents in **44Ru** and **55Ru**. Moreover, it was hoped that differences in $\Delta\nu_{C=O}$ for the excited-state complexes might be used to compare the extent of delocalization in the MLCT excited state for the two complexes. Ground-state infrared spectra of **44Ru** and **55Ru** (CD_3CN solution) feature a band at 1629 cm^{-1}, which is assigned to $\nu_{C=O}$ for the amide groups. Unfortunately, TRIR experiments carried out in the same solvent revealed no detectable change in $\nu_{C=O}$ for the excited-state complexes. This result indicates that $\nu_{C=O}$ shifts by less than 3 cm^{-1} when the complexes are in the MLCT excited state. In view of the fact that $\Delta\nu_{C=O} = -15$ cm^{-1} for $[Ru(bpy)_2(4,4'\text{-}(CONEt_2)_2bpy)]^{2+}$, this result suggests in **44Ru** and **55Ru** there is comparatively little added charge density in the phenylene rings when the complexes are in the MLCT excited state. An alternative explanation is that due to orbital delocalization in the PE−bpy ligands, the charge buildup at the amido carbonyl groups in the MLCT state is insufficient to give rise to a measurable shift in $\nu_{C=O}$.

Excited-State Delocalization in the PE-Substituted Complexes. It is clear that in **44Ru** and **55Ru** in the MLCT state the excited electron is localized on the PE substituted ligand. This conclusion is substantiated by the PL and transient absorption results, which indicate that the properties of the excited-state correlate with the structure and LUMO energy of the PE substituted ligands. It less clear, however, to what extent the excited electron is delocalized into the PE substituents, and whether the extent of delocalization is greater when the substituents are in the 4,4′- or 5,5′-positions on the bpy ligand.

Electrochemistry of **44Ru** and **55Ru** indicates that the PE substituents decrease the LUMO energy of the bpy ligand. Furthermore, the LUMO stabilization is markedly greater when

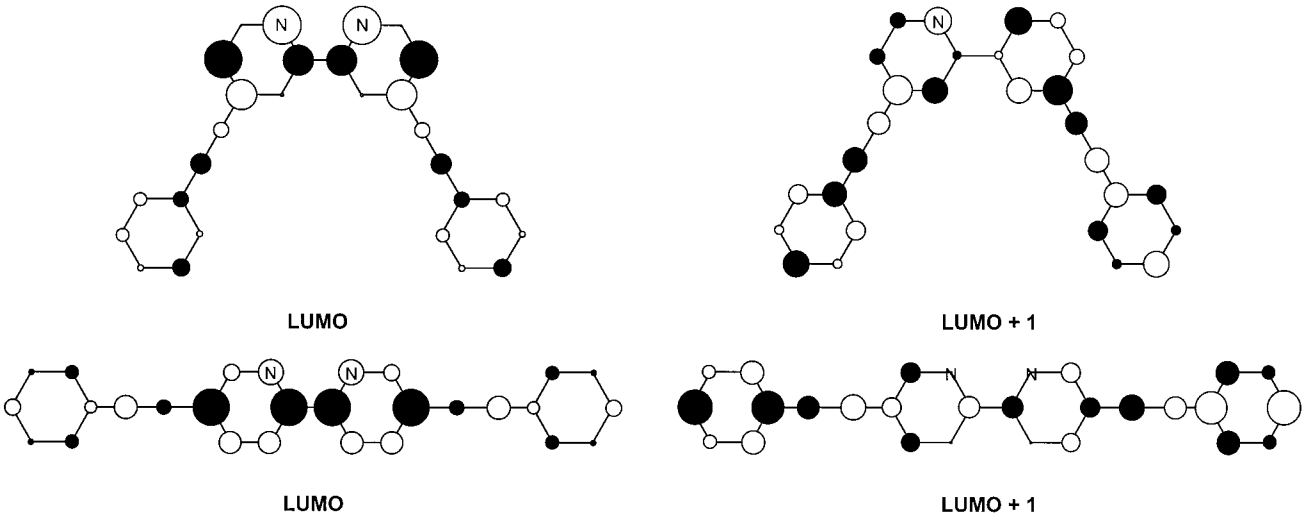

Figure 5. Graphical display of p_z orbital coefficients for LUMO and LUMO+1 molecular orbitals for **44L** and **55L**. Calculated using Hartree−Fock SCF theory using the STO-3G basis set.

the PE substituents are in the 5,5′-positions. This is not surprising, because with respect to the π-system of the PE substituted bpy ligand, the conjugation length is greater for **55L** than for **44L**. Improved π-conjugation in **55L** is a natural consequence of the fact that the pyridyl rings in the π-system are 1,4-substituted. By contrast, in **44L** the π-system is disrupted by the 1,3- (or "meta") pattern of substitution on the pyridine rings. The increased conjugation length (and concomitant lowering of the LUMO energy) in **55L** is clearly signaled by the fact that this compound features a lower energy π,π^* absorption and fluorescence.

All of the available evidence suggests that the LUMO in **55L** is more strongly delocalized than in **44L**. However, despite this fact, the photophysical data on **44Ru** and **55Ru** imply that in the MLCT state the excited electron is more delocalized in **44Ru**. First, the oscillator strength of the Ru → **44L** transition in **44Ru** is significantly larger than that of the Ru → **55L** transition in **55Ru**. It is also larger than that of the Ru → bpy MLCT transition in $Ru(bpy)_3^{2+}$. In addition, the radiative decay rate is enhanced in **44Ru**. These features imply that the MLCT transition dipole is larger in **44Ru** compared to that in **55Ru** and $Ru(bpy)_3^{2+}$, a result which strongly implies that delocalization into the PE substituents occurs in **44Ru**. (It is important to note that because the axis of π-conjugation in **55L** is perpendicular to the MLCT transition dipole, a priori the transition dipole moment is not expected to be enhanced in this complex by conjugation into the PE substitutents.) Second, the low-temperature PL spectra clearly indicate that electron vibrational coupling is lower in **44Ru** compared to that of **55Ru** and other Ru−polypyridyl complexes with similar excited-state energies.[8,48] In addition, the nonradiative decay rate is low in **44Ru**, again compared to **55Ru** and other ruthenium(II) complexes.[8,48] Several groups have argued that enhanced delocalization in the MLCT state gives rise to decreased electron-vibrational coupling, and this in turn leads to a decrease in the nonradiative decay rate.[5,6,8] This effect may be manifested in **44Ru** and to a lesser extent in **55Ru**.

Taken together, the results imply that delocalization in the MLCT state is greater in **44Ru** than in **55Ru**. In an attempt to understand this difference, molecular orbital calculations were carried out on the free ligands **44L** and **55L**. The calculations were carried out on the neutral free ligands using Hartree−Fock SCF theory with a minimal basis set (STO-3G). The objective of these calculations was to provide insight concerning the structure of the low-energy π^* orbitals on each ligand, since it is believed that these orbitals are the "acceptors" for the dπ (Ru) → π^* (**44L** or **55L**) MLCT transition. Figure 5 illustrates the coefficients of the p_z orbitals on the C and N atoms for the LUMO and (LUMO+1) orbitals of each ligand. The symmetry of the LUMO is the same in each ligand (B_1 in C_{2v} local symmetry) and is correct for overlap with the Ru d_{xz} orbital (which also transforms B_1 in C_{2v} local symmetry). This pattern follows for the (LUMO+1) orbitals on each ligand, which feature A_2 symmetry, which would be appropriate for overlap with the Ru d_{yz} orbital (which transforms A_2 in C_{2v} local symmetry). Qualitatively, it is clear that in both cases the LUMO and (LUMO+1) orbitals are delocalized significantly into the PE substituents. On a more quantitative level, the degree of delocalization is virtually identical in both ligands. Focusing on the LUMO, as assessed by the sums of the squares of the p_z orbital coefficients in both ligands, 75% of the electron density in the LUMO is centered on the bpy unit and 25% is delocalized into the PE substituents. Thus, by this measure, one would expect the degree of delocalization to be the same in each ligand. However, close inspection of the LUMO and (LUMO+1) orbitals reveals one important distinction between **44L** and **55L**. In **44L** the p_z coefficient on the pyridine nitrogen atoms is significantly larger in both the LUMO and (LUMO+1) orbitals. Indeed, the difference in the nitrogen p_z coefficients in the LUMO+1 is striking: 0.26 in **44L** vs 0.02 in **55L**. This difference is significant, because in the Mulliken charge transfer theory, the degree of charge transfer is directly proportional to the overlap between the orbitals localized on the donor and acceptor moieties.[9,36,42] Since the nitrogen atoms are the point of overlap between the π-system of the acceptor ligands and the metal-centered orbitals, the overlap depends strongly upon the coefficient of the p_z orbital on the nitrogen atoms. On this basis we believe that the MO calculations point to the possible origin of the difference in charge delocalization between **44Ru** and **55Ru**, that is, overlap between the Ru-based dπ orbitals and the π-electron system is greater in the former complex. This difference in overlap stems from the difference in structure of the low-energy π^* orbitals, which in turn is related to the geometry of the ligands. In essence, metal−ligand orbital overlap in **44Ru** is improved by the spatial distribution of the low-energy π^* orbitals on the PE-substituted ligand.

An important outcome of this study is that it demonstrates that although the effect of substituents on the energy of the π^*

orbital in 2,2′-bipyridine is stronger when these substituents are in the 5,5′-positions, the effect of π-delocalization in the MLCT state is *greater* when the π-acceptor substituents are located in the 4,4′-positions. Both of these effects stem from the spatial distribution of the low-energy π^* orbitals on the 2,2′-bipyridine unit. Thus, in the LUMO the orbital coefficients are larger on the 5,5′-positions, which enhances the electronic effect of substituents located in these positions. By contrast, the degree of metal to ligand charge transfer is strongly modulated by the size of the orbital coefficient on nitrogen,[9,36,42] and our MO calculations indicate that the presence of a π-acceptor in the 4,4′-positions leads to enhancement of the coefficient of the p_z nitrogen orbital, which in turn enhances the degree of charge transfer in the MCLT state. We believe that these effects are generalizable to any ligand substituents that function as π-acceptors.

Conclusion

A detailed photophysical study has been carried out on the complexes **44Ru** and **55Ru**. These complexes feature a lowest excited state that is based on dπ (Ru) $\rightarrow \pi^*$ (**44L** or **55L**) metal-to-ligand charge transfer. The presence of the PE substituents has a marked effect on the absorption, photoluminescence, and transient absorption spectra of the complexes. There is clear evidence that in the MLCT state the excited electron is delocalized into the PE-substituents. Moreover, the data also imply that the extent of delocalization is stronger in **44Ru**, that is, when the PE substituents are in the 4,4′-positions on the bpy unit. This is interesting, in view of the fact that the LUMO level is lower in **55L**, a feature that implies that the extent of intraligand delocalization is larger in this ligand. Molecular orbital calculations imply that the extent of delocalization in the MLCT state is related to the overlap between the low-energy π^* orbitals localized on the ligand with the metal-centered d orbitals. The overlap is strongly dependent on the size of the π^* orbital coefficients on the pyridine nitrogens, which in turn is modulated by the pattern of substituents on the bpy unit. We conclude that in general, π-acceptor substituents that are positioned in the 4,4′-positions will induce stronger delocalization in the MLCT excited state.

Acknowledgment. We gratefully acknowledge support from the National Science Foundation (Grant No. CHE-9901862) for support of this work.

Supporting Information Available: Mass and ^{1}H NMR spectra of **44L**, **55L**, **44Ru**, and **55Ru**, fitted photoluminescence spectra of **44Ru** and **55Ru**, and temperature-dependent emission lifetimes of **44Ru** and **55Ru**. This material is available free of charge via the Internet at http://pubs.acs.org.

References and Notes

(1) Caspar, J. V.; Meyer, T. J. *J. Phys. Chem.* **1983**, *87*, 952−957.
(2) Juris, A.; Balzani, V.; Barigelletti, F.; Campagna, S.; Belser, P.; von Zelewsky, A. *Coord. Chem. Rev.* **1988**, *84*, 85−277.
(3) Worl, L. A.; Duesing, R.; Chen, P.; Della Ciana, L.; Meyer, T. J. *J. Chem. Soc., Dalton Trans.* **1991**, 849−858.
(4) Schanze, K. S.; Macqueen, D. B.; Perkins, T. A.; Cabana, L. A. *Coord. Chem. Rev.* **1993**, *122*, 63−89.
(5) Strouse, G. F.; Schoonover, J. R.; Duesing, R.; Boyde, S.; Jones, W. E., Jr.; Meyer, T. J. *Inorg. Chem.* **1995**, *34*, 473−487.
(6) Treadway, J. A.; Loeb, B.; Lopez, R.; Anderson, P. A.; Keene, F. R.; Meyer, T. J. *Inorg. Chem.* **1996**, *35*, 2242−2246.
(7) Grosshenny, V.; Harriman, A.; Romero, F. M.; Ziessel, R. *J. Phys. Chem.* **1996**, *100*, 17472−17484.
(8) Damrauer, N. H.; Boussie, T. R.; Devenney, M.; McCusker, J. K. *J. Am. Chem. Soc.* **1997**, *119*, 8253−8268.
(9) Mines, G. A.; Roberts, J. A.; Hupp, J. T. *Inorg. Chem.* **1992**, *31*, 125−126.
(10) Ley, K. D.; Whittle, C. E.; Bartberger, M. D.; Schanze, K. S. *J. Am. Chem. Soc.* **1997**, *119*, 3423−3424.
(11) Ley, K. D.; Li, Y. T.; Johnson, J. V.; Powell, D. H.; Schanze, K. S. *Chem. Commun.* **1999**, 1749−1750.
(12) Li, Y. T.; Whittle, C. E.; Walters, K. A.; Ley, K. D.; Schanze, K. S. *Pure Appl. Chem.* **2001**, *73*, 497−501.
(13) Walters, K. A.; Ley, K. D.; Cavalaheiro, C. S. P.; Miller, S. E.; Gosztola, D.; Wasielewski, M. R.; Bussandri, A. P.; van Willigen, H.; Schanze, K. S. *J. Am. Chem. Soc.* **2001**, *123*, 8329−8342.
(14) Wong, C. T.; Chan, W. K. *Adv. Mater.* **1999**, *11*, 455−459.
(15) Wang, J.; Wang, R.; Yang, J.; Zheng, Z.; Carducci, M. D.; Cayou, T.; Peyghambarian, N.; Jabbour, G. E. *J. Am. Chem. Soc.* **2001**, *123*, 6179−6180.
(16) Bernier, P., Lefrant, S., Bidan, G., Eds. *Advances in Synthetic Metals. Twenty Years of Progress in Science and Technology*; Elsevier Science SA: Amsterdam, 1999.
(17) Peng, Z.; Gharavi, A. R.; Yu, L. *J. Am. Chem. Soc.* **1997**, *119*, 4622−4632.
(18) Wang, Q.; Wang, L.; Yu, L. *J. Am. Chem. Soc.* **1998**, *120*, 12860−12868.
(19) Li, Y.; Whittle, C. E.; Walters, K. A.; Ley, K. D.; Schanze, K. S. *MRS Symp. Proc.*, in press.
(20) Chen, P. Y.; Omberg, K. M.; Kavaliunas, D. A.; Treadway, J. A.; Palmer, R. A.; Meyer, T. J. *Inorg. Chem.* **1997**, *36*, 954−955.
(21) Omberg, K. M.; Smith, G. D.; Kavaliunas, D. A.; Chen, P.; Treadway, J. A.; Schoonover, J. R.; Palmer, R. A.; Meyer, T. J. *Inorg. Chem.* **1999**, *38*, 951−956.
(22) Grosshenny, V.; Ziessel, R. *Tetrahedron Lett.* **1992**, *33*, 8075−8078.
(23) Grosshenny, V.; Romero, F. M.; Ziessel, R. *J. Org. Chem.* **1997**, *62*, 1491−1500.
(24) Wolfe, J. P.; Buchwald, S. L. *J. Org. Chem.* **1996**, *61*, 1133−1135.
(25) Sessler, J. L.; Brown, C. T.; Wang, R.; Hirose, T. *Inorg. Chim. Acta* **1996**, *251*, 135−140.
(26) Sullivan, B. P.; Salmon, D. J.; Meyer, T. J. *Inorg. Chem.* **1978**, *17*, 3334−3341.
(27) Harriman, A. *J. Chem. Soc., Chem. Commun.* **1977**, 777−778.
(28) Caspar, J. V. Ph.D. Dissertation, University of North Carolina, Chapel Hill, NC, 1982.
(29) Wang, Y.; Schanze, K. S. *Chem. Phys.* **1993**, *176*, 305−319.
(30) Omberg, K. M.; Schoonover, J. R.; Treadway, J. A.; Leasure, R. M.; Dyer, R. B.; Meyer, T. J. *J. Am. Chem. Soc.* **1997**, *119*, 7013−7018.
(31) Omberg, K. M.; Schoonover, J. R.; Meyer, T. J. *J. Phys. Chem. A* **1997**, *101*, 9531−9536.
(32) Lakowicz, J. R. *Principles of Fluorescence Spectroscopy*, 2nd ed.; Kluwer Academic/Plenum Publishers: Dordrecht, The Netherlands, 1999.
(33) Gennett, T.; Milner, D. F.; Weaver, M. J. *J. Phys. Chem.* **1985**, *89*, 2787−2794.
(34) Sahami, S.; Weaver, M. J. *J. Electroanal. Chem.* **1981**, *122*, 155−170.
(35) Schmidt, M. W.; Baldridge, K. K.; Boatz, J. A.; Elbert, S. T.; Gordon, M. S.; Jensen, J. H.; Koseki, S.; Matsunaga, N.; Nguyen, K. A.; Su, S. J.; Windus, T. L.; Dupuis, M.; Montgomery, J. A. *J. Comput. Chem.* **1993**, *14*, 1347−1363.
(36) Walters, K. A.; Premvardhan, L. L.; Liu, Y.; Peteanu, L. A.; Schanze, K. S. *Chem. Phys. Lett.* **2001**, *339*, 255−262.
(37) Walters, K. A. Ph.D. Dissertation, University of Florida, Gainesville, FL, 2000.
(38) Zhu, S. S.; Kingsborough, R. P.; Swager, T. M. *J. Mater. Chem.* **1999**, *9*, 2123-2131.
(39) Ziener, U.; Godt, A. *J. Org. Chem.* **1997**, *62*, 6137−6143.
(40) Grummt, U. W.; Birckner, E.; Klemm, E.; Egbe, D. A. M.; Heise, B. *J. Phys. Org. Chem.* **2000**, *13*, 112−126.
(41) Manas, E. S.; Chen, L. X. *Chem. Phys. Lett.* **2000**, *331*, 299−307.
(42) Phifer, C. C.; McMillin, D. R. *Inorg. Chem.* **1986**, *25*, 1329−1333.
(43) Wrighton, M.; Morse, D. L. *J. Am. Chem. Soc.* **1974**, *96*, 998−1003.
(44) Lees, A. J. *Chem. Rev.* **1987**, *87*, 711−743.
(45) Kober, E. M.; Caspar, J. V.; Lumpkin, R. S.; Meyer, T. J. *J. Phys. Chem.* **1986**, *90*, 3722−3734.
(46) Van Houten, J.; Watts, R. *J. Am. Chem. Soc.* **1976**, *98*, 4853−4858.
(47) Wacholtz, W. F.; Auerbach, R. A.; Schmehl, R. H. *Inorg. Chem.* **1986**, *25*, 227−234.
(48) Barqawi, K. R.; Murtaza, Z.; Meyer, T. J. *J. Phys. Chem.* **1991**, *95*, 47−50.
(49) Ohno, T.; Yoshimura, A.; Prasad, D. R.; Hoffman, M. Z. *J. Phys. Chem.* **1991**, *95*, 4723−4728.
(50) Watts, R. J. *J. Chem. Educ.* **1983**, *60*, 834−842.

(51) The spectra for the two complexes were obtained at the same laser power and with samples having the same ground-state absorptivity at the excitation wavelength.

(52) Sun, H.; Hoffman, M. Z.; Mulazzani, Q. G. *Res. Chem. Intermed.* **1994**, *20*, 735−754.

(53) Chen, P.; Danielson, E.; Meyer, T. J. *J. Phys. Chem.* **1988**, *92*, 3708−3711.

(54) Stern−Volmer luminescence quenching experiments were carried out using DMA. Both **44Ru** and **55Ru** were quenched efficiently, and the following bimolecular quenching constants were extracted from the quenching data: k_q(**44Ru**) = 5.2 × 10^8 M^{-1} s^{-1}; k_q(**55Ru**) = 1.8 × 10^9 M^{-1} s^{-1}.

(55) Zhang, X. M.; Yeh, S. R.; Hong, S.; Freccero, M.; Albini, A.; Falvey, D. E.; Mariano, P. S. *J. Am. Chem. Soc.* **1994**, *116*, 4211−4220.

(56) The low-temperature absorption spectra feature a tailing baseline on the long wavelength side of the MLCT bands. This feature is due to light scattering that arises because the samples are contained in an optical cryostat and consequently the light beam passes through four windows.

(57) Blakley, R. L.; Myrick, M. L.; DeArmond, M. K. *Inorg. Chem.* **1988**, *27*, 589−590.

(58) Schoonover, J. R.; Strouse, G. F. *Chem. Rev.* **1998**, *98*, 1335−1355.